


RESEARCH

Open Access



Effect of various additives on aluminum oxide thin films prepared by dip coating, thermal behavior, kinetics and optical properties

Mohammed Bouzbib^{1*} , Maryam El Marouani² and Katalin Sinkó³

Abstract

Aluminum oxide thin films attract research interest due to their properties. Aluminum acetate was used as an Al source with acetic acid, oxalic acid, and nitric acid as additives. The transmittance and the thickness of the films strongly depend on the additives, with the approximate bandgap energy changing from 5 eV to 5.4 eV. The aluminum oxide film deposited by dip-coating is presented great uniform surface morphology. The knowledge of the degradation kinetics of materials is essential for investigating the thermal stability of compounds. The acetic acid thin film proved to be the most efficient additive by demonstrating interesting optoelectronic properties. The thin films deposited by dip-coating were characterized by using X-ray grazing incidence diffraction, SEM, UV-Visible spectroscopy. Gamma aluminum oxide thin films prepared by acetic acid can be a good candidate for a wide range of optical applications.

Keywords: Al₂O₃, Thin films, Dip coating, Optical properties, Additives

Introduction

Aluminum oxide thin films (Al₂O₃) exhibits several interesting properties [1, 2], such as high optical transparency [3], high abrasive and corrosion resistance [4, 5], high chemical and thermal stability [6], and wide band-gap [7]. Due to the mentioned properties, aluminum oxide thin films possess a wide range of applications in optoelectronics and microelectronics devices serving as insulating [8], hard protective layers [9], surface passivation e.g. for silicon solar cells [10].

The crystalline structure of Al₂O₃ can take many different forms, including: α , γ , χ , η , θ , κ , δ and ρ [11].

Among these transformations, γ -Al₂O₃ is a significant material that is employed in a variety of applications, including catalytic substrates in the automotive and

petroleum sectors, composite materials for spacecraft, and abrasive and thermal wear coatings [12].

The method of deposition and the temperature of the substrate are frequent factors in the creation of these phases. At low temperatures, the amorphous phase occurs, the γ -alumina phase takes over at intermediate temperatures, and the κ and α -Al₂O₃ phases grow at high temperatures [13].

There are various chemical and physical methods applied to prepare aluminum oxide thin films such as chemical vapor deposition (CVD) [14], atomic layer deposition (ALD) [15], Pulsed laser deposition (PLD) [16, 17], spray pyrolysis (SP) [18–20], magnetron sputtering [16, 21], anodization [22–24] spin coating [25], and dip coating [26–28]. Dip-coating was used due to simplicity, low cost, and the ability to produce high-quality films, and it is widely utilized for the deposition of oxide thin films [25].

* Correspondence: mbouzbib@caesar.elte.hu;
mohammedbouzbib@gmail.com

¹ Doctoral School of Environmental Sciences, Eötvös Loránd University, Budapest H-1117, Hungary
Full list of author information is available at the end of the article

This work aims to investigate the solvent effect on the structural, optical, and morphological properties of aluminum oxide thin film by changing different solvents. The degradation kinetics of materials is essential for investigating the thermal stability of compounds. Degradation kinetics can be studied by several methods but one of the most popular and simplest techniques widely used in the literature is the thermogravimetric analysis [29].

The morphology of the films has been investigated by grazing incidence X-ray diffraction (GIXRD), the quality of the film by scanning electron microscopy (SEM). The optical properties of aluminum oxide thin films deposited by dip-coating were characterized by UV-visible spectrophotometry. The degradation kinetics of materials was determined by thermogravimetry (TG) techniques.

Materials and methods

Preparation

The aluminum oxide thin films synthesis process is shown in (Fig.1). the starting solution was prepared by dissolving the aluminum acetate $\text{Al}(\text{OH})(\text{C}_2\text{H}_3\text{O}_2)_2$ (Sigma-Aldrich, at) in NaOH (Molar, at) solution under an air atmosphere with 0.11 M ratio of OH to Al, the mixed solution was continuously stirred at 55 °C for 1 h.

To dissolve the basic aluminum acetate, various acids (nitric acid, acetic acid, and oxalic acid) were added to the basic solution to get pH = 7. The acids initialize the

precipitation and stabilize the sol system [25, 26]. The acetic acid received an emphasized attention, the acetic acid plays an important role as a bidentate ligand between two Al ions furthering the formation of a 3D network [30].

IGEPAL CO-520 or poly (oxyethylene) nonylphenyl ether) (Sigma-Aldrich) was added as a non-ionic surfactant to the colloid solution to improve the connection between layer and substrate [31]. Thin films were deposited by a dip coating method on quartz substrate at room temperature with a constant speed (5 cm/min) by an automated dip-coater (PTL-MM01 Dip Coater). The substrates were ultrasonically cleaned with acetone, ethanol, and deionized water dried. After coating the samples were dried at 70 °C for 1 h and then heated at 600 °C for 3 h with a heating rate of 2 °C/min (Fig.2). the aluminum oxide thin films synthesis process is shown in (Fig.1).

Kinetic approach

There are several approaches for estimating kinetic parameters from thermogravimetric data. It is therefore essential to specify the approach adopted in any kinetic exploitation of the experimental mass loss data. In this work, the kinetic parameters are determined by the Coats Redfern method. The expression to achieve these parameters is obtained from the reaction rate. Thus, in the kinetic analysis of thermal decomposition reactions,

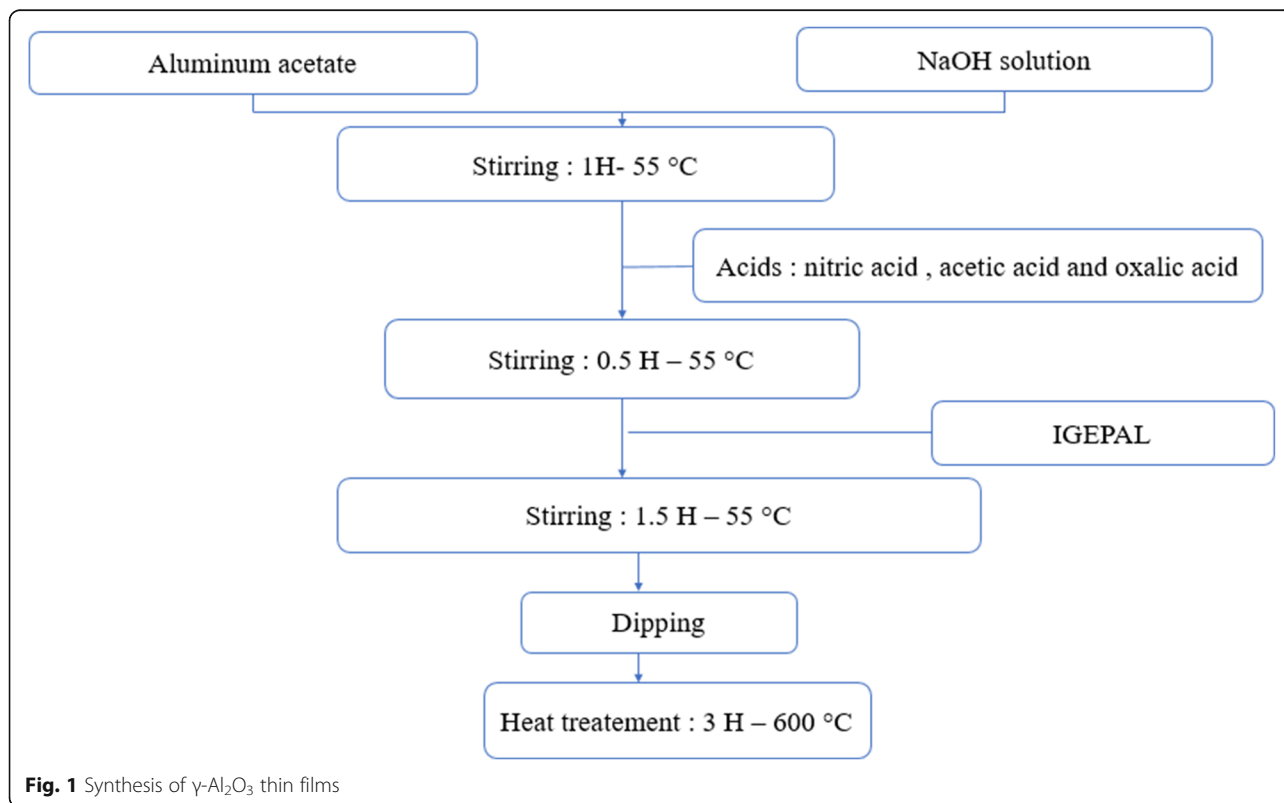


Fig. 1 Synthesis of $\gamma\text{-Al}_2\text{O}_3$ thin films

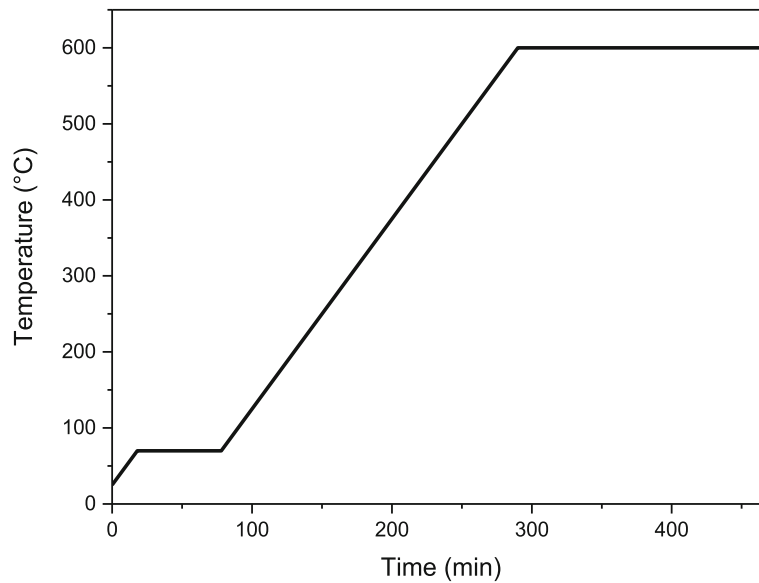


Fig. 2 Schematically graph of heat treatment of gamma aluminum oxide thin films

Table 1 Thermal degradation modes proposed for gas-solid reactions [32–34]

Degradation mode	Code	Differential form: $f(a)$	Integral form: $g(a)$
Diffusion			
One-way transport	D1	$1 / (2a)$	a^2
two-way transport, Valensi-Barrer	D2	$-1 / \ln(1-a)$	$a + (1-a)\ln(1-a)$
three-way transport, Jander	D3	$1,5(1-a)^{2/3} / [1-(1-a)^{1/3}]$	$[1-(1-a)^{1/3}]^2$
Ginstling-Brounshtein	D4	$1,5 / [(1-a)^{-1/3}-1]$	$1-2a/3-(1-a)^{2/3}$
Zhuravlev	D5	$1,5(1-a)^{2/3} / [1 / (1-a)^{1/3}-1]$	$[1 / (1-a)^{1/3}-1]^2$
Anti-Jander	D6	$1,5(1+a)^{2/3} / [(1+a)^{1/3}-1]$	$[(1+a)^{1/3}-1]^2$
Kroger-Ziegler	D7	$[1,5(1-a)^{2/3} / [1-(1-a)^{1/3}]] / t$	$[1-(1-a)^{1/3}]^2 - \log(t)$
Two dimensions, Jander	D8	$(1-a)^{1/2} / [1-(1-a)^{1/2}]$	$[1-(1-a)^{1/2}]^2$
Two dimensions, Anti-Jander	D9	$(1+a)^{1/2} / [(1+a)^{1/2}-1]$	$[(1+a)^{1/2}-1]^2$
Interfacial transfer	D10	$3(1-a)^{4/3}$	$[1 / (1-a)^{1/3}-1]$
Transfer and diffusion	D11	$3 / [(1-a)^{-4/3} - (1-a)^{-1}]$	$1/(1-a)^{1/3}-1 + 1/3\ln(1-a)$
Diffusion with two directions	D12	$3 / [(1-a)^{-8/3} - (1-a)^{-7/3}]$	$1/5(1-a)^{-5/3} - 1/4(1-a)^{-4/3} + 1/20$
Random nucleation and nuclei growth			
Avrami-Erofeev [36] $n = 1, 2, 3, 4$ et 5	An	$x(1-a)[- \ln(1-a)]^y$ $x = 4, 2, 3, 4/3$ and $3/2$ $y = 3/4, 1/2, 2/3, 1/4$ and $1/3$	$[- \ln(1-a)]^z$ $z = 1/4, 1/2, 1/3, 3/4$ and $2/3$
Chemical reactions			
Zero order	F0	Constant	a
First order	F1	$1-a$	$-\ln(1-a)$
Second order	F2	$(1-a)^2$	$(1-a)^{-1}-1$
Contraction (surface, volume and interface respectively for $n = 2, 3$ and 4)	Rn	$x(1-a)^y$ $x = 2, 3$ et $3/2$. $y = 1/2, 2/3$ and $1/3$	$1-(1-a)^z$ $z = 1/2, 1/3$ and $2/3$
Power / Exponential			
Low power (half, third and quarter respectively for $n = 2, 3$ and 4)	Pn	na^x $x = 1/2, 2/3$ and $3/4$	a^y $y = 1/2, 1/3$ et $1/4$
Exponential	E1	a	$\ln(a)$

the reaction rate is written according to the following form:

$$\frac{d\alpha}{dt} = kf(\alpha) \quad (1)$$

Where α is a characteristic variable of reaction progress, related to the mass of the sample m by the formula:

$$\alpha = \frac{m_0 - m_t}{m_0 - m_f} \quad (2)$$

Where, m_0 is the initial weight of the sample, m_t is the weight of the sample at the particular temperature T , and m_∞ is the weight at the end of degradation step, $f(\alpha)$ represents the mode of degradation of the substance. The function $f(\alpha)$ does not depend on the temperature but rather on the degradation mode of the subjected matter.

The different modes proposed in the literature [32–34] are grouped in Table 1. In this same Table, the function $g(\alpha) = \int_0^\alpha \frac{d\alpha}{f(\alpha)}$ represents the integral form of the function $f(\alpha)$ [35].

k is the reaction rate constant. It is accepted that k following the Arrhenius law:

$$k = A \exp\left(\frac{-E}{RT}\right) \quad (3)$$

Where E is the apparent activation energy in kJ/mol, R is the perfect gas constant in Joules. $K^{-1} \cdot mol^{-1}$, A is the pre-exponential factor or frequency factor in min^{-1} , T is the absolute temperature in $^{\circ}K$,

A , E and $f(\alpha)$ are called the kinetic triplets of a reaction.

D_1, D_2, \dots are symbols given to models.

Procedure for kinetic parameters determination

In order to determine the kinetic parameters of our samples, the Coats–Redfern method [29], which is given in Eq. 4, is expressed as follows:

$$\ln\left(\frac{g(\alpha)}{T^2}\right) = \ln\frac{AR}{\beta E_a} - \frac{E_a}{RT} \quad (4)$$

Where α is a characteristic variable of the reaction progress of the sample and T is the absolute temperature, $g(\alpha)$ represents functions commonly used for the description of thermal decomposition (Table 1). A is the frequency factor, E_a is the activation energy, R is the gas constant, and β is the heating rate.

A plot of $\ln(g(\alpha)/T^2)$ against $1/T$ will give a straight line of slope $-E/R$ and an intercept of $\ln(AR/\beta E)$ for an appropriate form of $g(\alpha)$. Thus, based on the correct form of $g(\alpha)$, the activation energy and the pre-

exponential factor could be respectively determined from the slope and intercept terms of the regression line.

Table 1 lists the most common kinetic $g(\alpha)$ functions, which were used in this study for the estimation of reaction mechanisms from dynamic TG curves by using Coats–Redfern method.

Investigation methods

Scanning electron microscopy (SEM): The surface covering, and the layer thickness has been studied by a FEI Quanta 3D FEG scanning electron microscope (SEM). The SEM images were prepared by the Everhart-Thornley secondary electron detector (ETD), its ultimate resolution is 1–2 nm. Since the conductance of the particles investigated is high enough to remove the electric charge accumulated on the surface, the SEM images were performed in a high vacuum without any coverage on the specimen surface. For the best SEM visibility, the particles were deposited on a HOPG (graphite) substrate surface. SEM combined with energy disperse X-ray spectroscopy (EDX) is applied for spatially resolved chemical analysis of layers.

Grazing incidence X-ray diffraction (GIXRD) measurements were performed by a Rigaku Smartlab X-ray diffractometer equipped with a 1.2 kW copper source (radiation wavelength: $CuK\alpha$; $\lambda = 0.15418$ nm). To reduce the effect of the substrate, a grazing incidence parallel-beam geometry was used with an incidence angle of $\omega = 1^{\circ}$. Scans were performed in the range 2θ between 10° – 110° with an 1D silicon strip detector (D/Tex ultra 250) by a speed $0.2^{\circ}/min$. The XRD data were collected over the 2θ range of 9° – 90° with a step size 0.005° . Identification of phases was performed by comparing the diffraction patterns with standard PDF cards.

UV–Visible spectroscopy: The transmittance of thin films was determined by UV–visible spectroscopy using Dynamica spectrophotometer with UV Detective program at room temperature, in the range of 200–1000 nm.

Thermogravimetric (TG) of bulk aluminum oxide were made on a simultaneous thermal analyzer of the "LabsysTMEvo (1F)" type and SETARAM brand. This device consists of a TG microbalance associated with DTA sensor with a single rod, a metal resistor furnace up to $1600^{\circ}C$, and multitasking software controlling the various modules. The tests are carried out from ambient temperature to $800^{\circ}C$ with a temperature rise rate of $7^{\circ}C min^{-1}$ under argon with a flow rate of $10 cm^3 \cdot min^{-1}$. The initial mass of the sample is about 10 mg.

Results and discussion

To determine the thermal behavior of the thin films derived from the aluminum acetate, thermogravimetry

(TG) was used. The TG curve for AlOOH sol obtained directly by the acetic acid treatment is shown in Fig. 3. The small weight loss that occurred at 148°C is mostly caused by desorption of the adsorbed moisture and solvent evaporation, while a large weight loss happens within the temperature range from 182°C to 540°C is due to the decomposition of the organic groups by the release of CO_2 and H_2O . No visible weight loss is detected at temperatures above 540°C , according to the results acquired, it is suitable to calcine the aluminum oxide thin films at 600°C . When compared to bulk aluminum oxide, the aluminum oxide colloidal sol showed a significant weight loss due to solvent evaporation at 148°C .

Figure 4 shows GIXRD patterns of the films annealed at 600°C with various additives. The crystallinity degree can be influenced by many factors such as precursor concentration, pH reaction, and solvents. The films show Bragg diffraction peaks ascribed to more or less ordered $\gamma\text{-Al}_2\text{O}_3$ crystalline phase. The quality of acids does not really affect crystallinity. These patterns show slight shifts with different acids.

Scanning electron microscope (SEM) was used to investigate the surface morphology and cross-section of the films as shown in Fig. 5. According to SEM images, the films morphology can be described by a uniform, with no cracks and a non-defective surface. Moreover, the smooth surface morphology decreased from acetic to nitric acid and oxalic acid. The complex formed between the acetate acid and aluminum ions helps to develop a

homogenous. The cross-sectional SEM images present layer thicknesses of approximately 90, 140 and 115 nm respectively.

The chemical composition of the thin film was determined by using EDX (Fig. 6). EDX analysis from five different areas indicates the presence of Al and oxygen-rich, beside silicon which is derived from quartz substrate of layer. The EDX confirms the efficient deposition of Al_2O_3 thin film.

To get information on the optical properties of the films, transmittance spectra of $\gamma\text{-Al}_2\text{O}_3$ films on quartz substrates were measured in the wavelength range from 200 to 1000 nm (Fig. 7). It can be noticed that the transmittance of the films is over 70% in the wavelength range from 400 to 1000 nm. The transmittance of the films decreased from acetic, nitric, and oxalic acid respectively which confirms that thickness has an inverse relation with transmittance [37], the high absorbance of gamma aluminum oxide prepared by oxalic acid can also be explained by light trapping due to their textured morphology [38]. The optical band gap relation with the absorption coefficient is given by the relation:

$$(ah\nu)^2 = C(h\nu - E_g) \quad (5)$$

Where α is absorption coefficient, C is a constant, h is Plank constant and E_g is the optical band gap. The band gap E_g can be determined by extrapolation from the

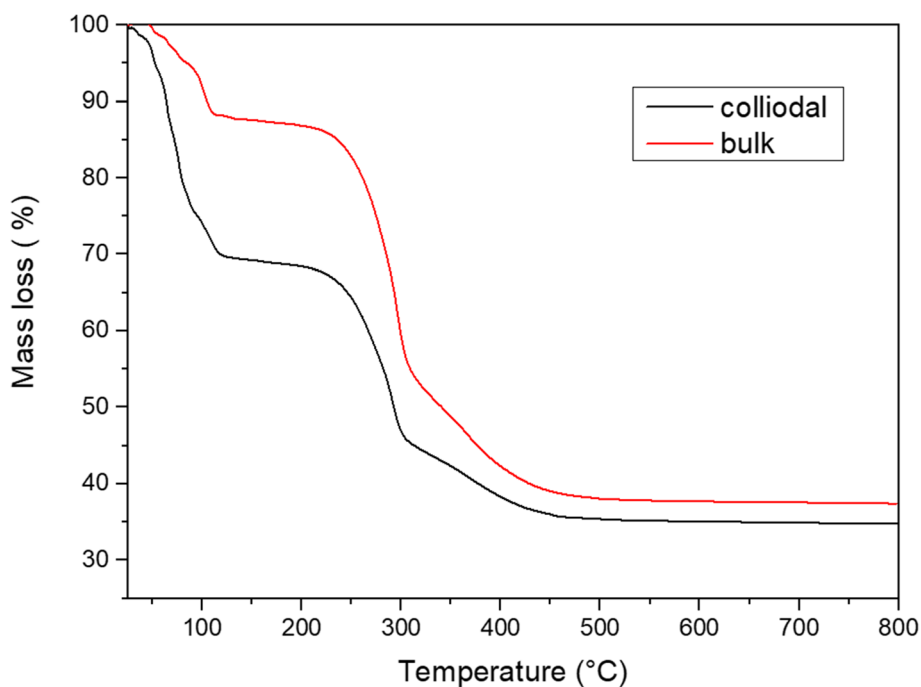


Fig. 3 Thermogravimetry (TG) of bulk aluminum oxide and colloidal sol

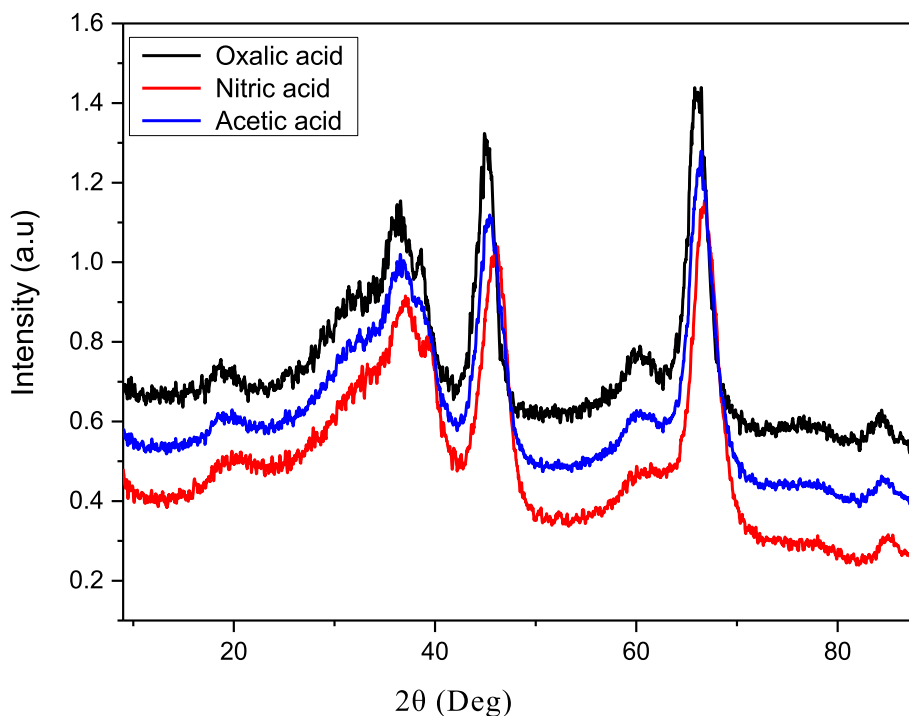


Fig. 4 Grazing incidence X-ray diffraction patterns of the films annealed at 600 °C with various acids (nitric acid, acetic acid, and oxalic acid)

linear portion of the curves till they intercept the photon energy axis (Table 2). Figure 8. The band gap values are given as 4.99, 5.21, and 5.34 eV for nitric acid, oxalic acid and acetic acid respectively. Band gap value can be change by some defect levels [39].

Thermal analysis

Thermogravimetric analysis (TGA-DTG)

Determination of the thermal behaviour of γ - Al_2O_3 thin films was carried out from the aluminum acetate, thermogravimetry (TG) was used. The TG curves for colloidal alumina sol is shown in Fig. 3. The small weight loss that occurred at 148 °C is mostly caused by the desorption of the adsorbed moisture and solvent evaporation. While, a large weight loss happens within the temperature range from 182 °C to ~310 °C is due to the decomposition of the organic groups (mainly acetate ions) by the release of CO_2 and H_2O molecules. Another escape of H_2O molecules up to 540 °C can be assigned to the transformation of AlOOH to Al_2O_3 . No detectable weight loss is above 540 °C.

Kinetic parameters estimation

To calculate and understand the nature of the decomposition, kinetic exploitation is made on a dynamic chemical regime assuming that the decomposition is a global reaction where physical limitation is neglected.

The complete thermogram was divided into distinct sections according to their degradation steps. Curves indicating the solid-state mechanisms of alumina degradation under an inert atmosphere are shown in Fig. 9. The values of activation energy E_a , pre-exponential factor A and correlation factors R^2 for the first and second degradation steps are listed in Table 3. Moreover, the parameters A and E are moving in the same direction and their values depend on the mode of degradation. The relationship between A and E_a , called the “apparent compensation effect” is often mentioned in the literature. Figure 10 shows traces of the values of $\ln A$ as a function of E_a . The effect of compensation is another way to further discrimination between degradation modes [40]. Thus, for the first region (second weight loss step in TGA thermogram), it was observed from Table 3 that the best correlation coefficients were obtained for F0, F1, F2, F3, R2, R3, P2, P3, D3, A2, and A3, with energy values running from 35.1 to 135.8 kJ/mol. Regarding, second degradation step (third weight loss step), degradation mechanisms that give the best mathematical fit for both samples were F1, F2, F3, R2, R3, D3 and A2, with values of activation energy from 7.154 to 121.25 kJ/mol. Likewise, results of the two regions show that the highest activation energies were found in the first thermal degradation regions where the main pyrolysis reaction took place and the

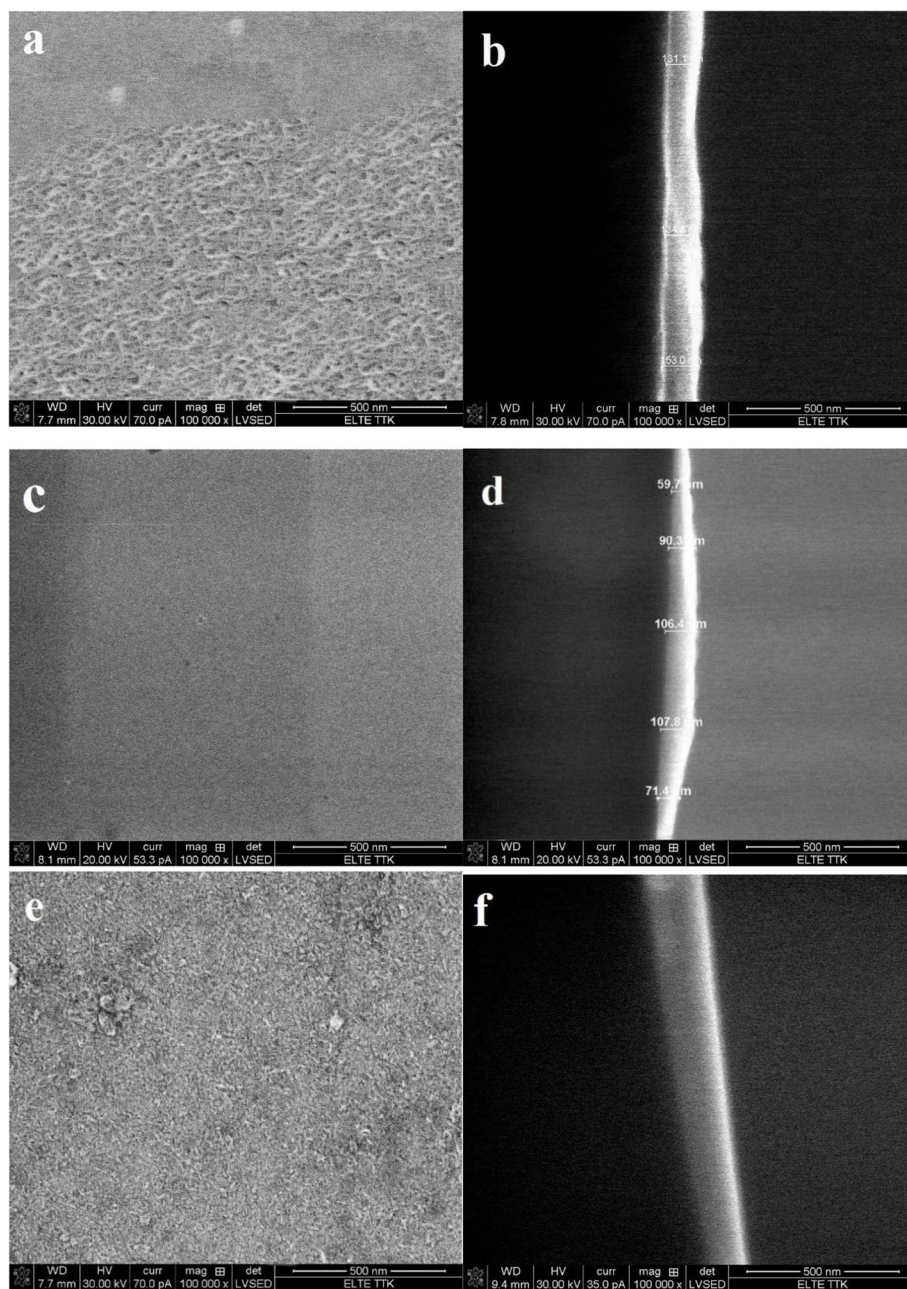


Fig. 5 Scanning electron microscopy of γ - Al_2O_3 thin films top view (a, c, e) respectively nitric acid, acetic acid, and oxalic acid), cross-section (b, d, f)

largest weight loss occurred. The values of the pre-exponential factor (Table 3) indicate that it depends on the degradation mode.

Conclusion

In this work, gamma aluminum oxide thin films were prepared by various solvents. The X-ray diffraction patterns of the films confirm the presence of γ - Al_2O_3 can be crystallized at a temperature of 600 °C. The optical

transparency of the films are over 70% in the wavelength range from 400 to 1000 nm with an average band gap value of 5.18 eV, therefore the γ - Al_2O_3 layer prepared by acetic acid shows the highest transmittance with the thinnest and smoothest surface morphology which can be relevant for many applications. The scanning electron microscopy presents a uniform no cracks and non-defective surface morphology. TGA curves indicate that active pyrolysis range is from 182 °C to 540 °C, where

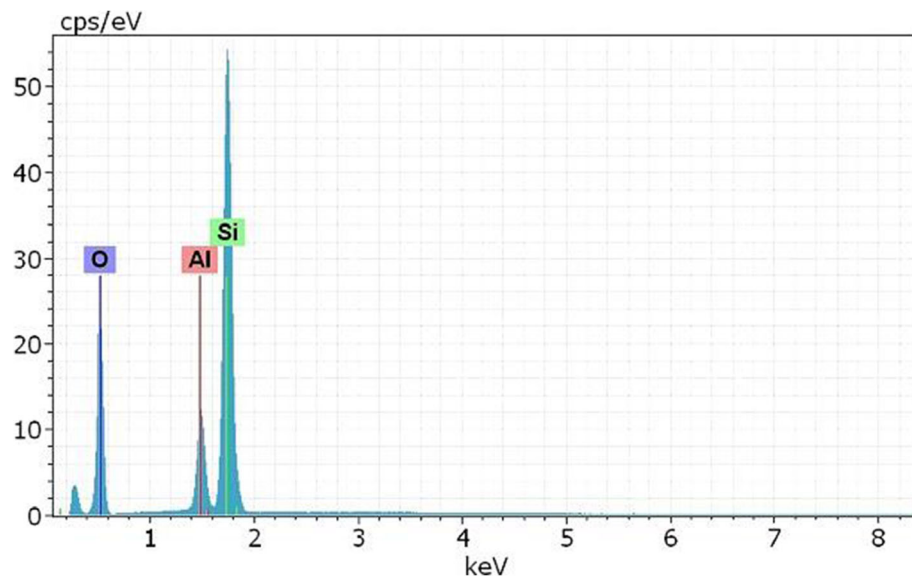


Fig. 6 EDX (Energy Dispersive X-ray) spectrum of Al_2O_3 thin films

the major decomposition of organic groups occur up to $\sim 310^\circ\text{C}$ and from $\sim 310^\circ\text{C}$ to 540°C AlOOH turns into Al_2O_3 . From about 400°C , γ -crystalline phase begins to form. The ideal temperature of final treatment is 600°C . The results of kinetics study shows that the highest activation energies were found in the first thermal

degradation region where the main pyrolysis reaction took place and the largest weight loss occurred, with values of activation energies running from 35.1 to 135.8 KJ/mol.

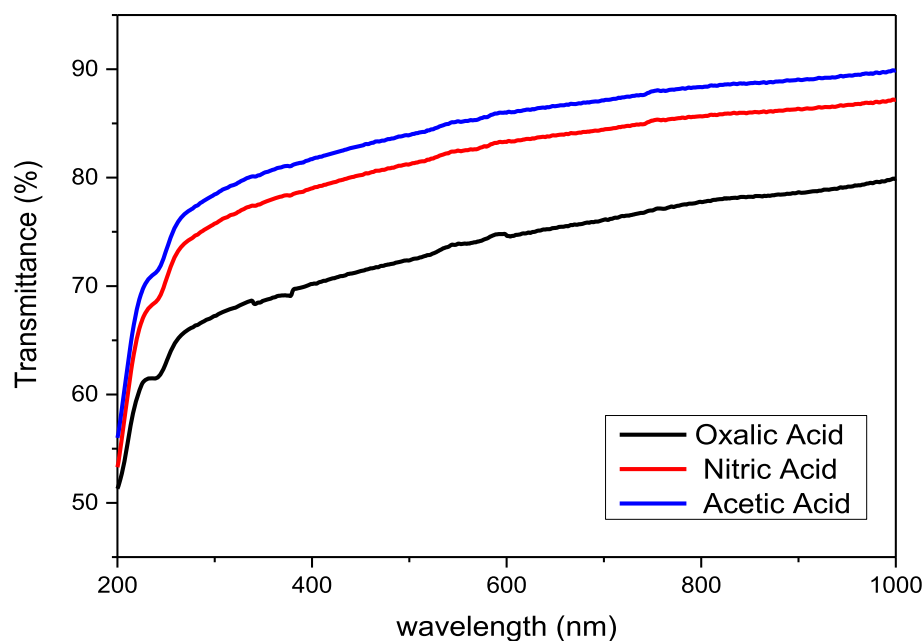


Fig. 7 Transmittance spectra of $\gamma\text{-Al}_2\text{O}_3$ films on quartz substrates with various acids (acetic acid, nitric acid and, oxalic acid)

Table 2 Optical band gaps of different thin films extracted from the Tauc plot

Sample	Eg (eV)
Thin film acetic acid	5.4
Thin film nitric acid	5
Thin film oxalic acid	5.3

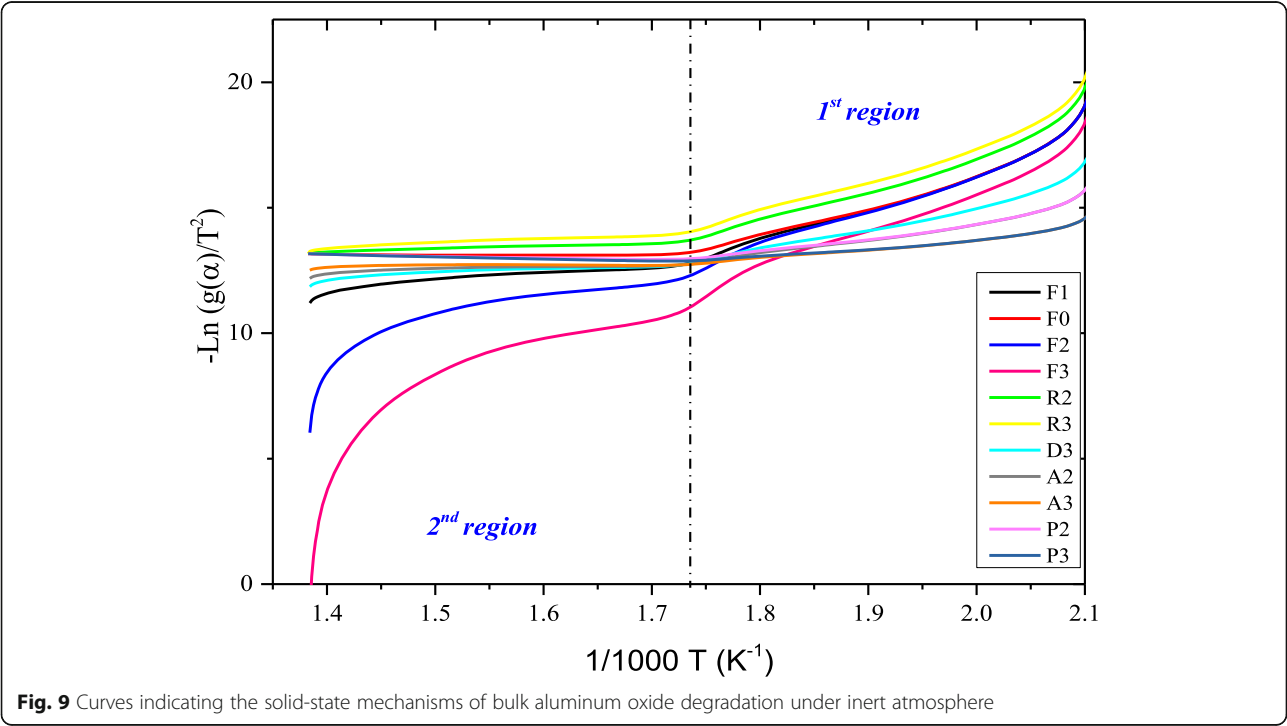
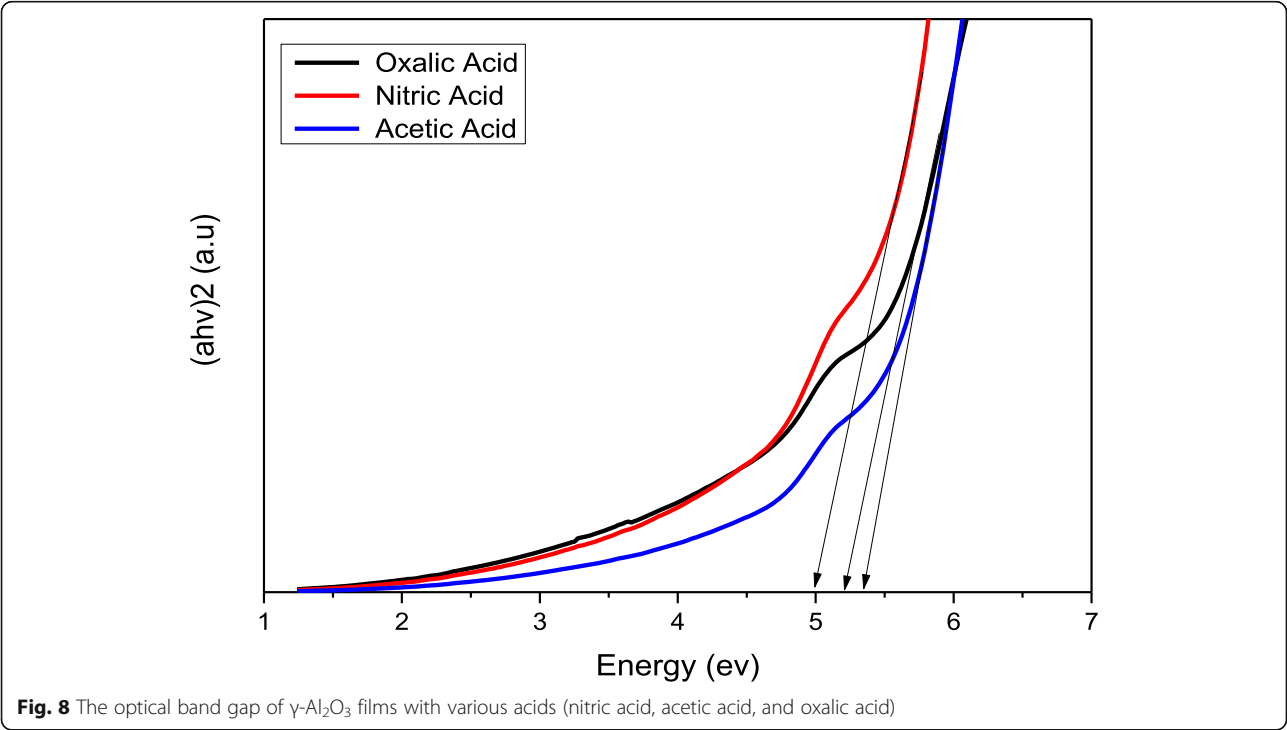
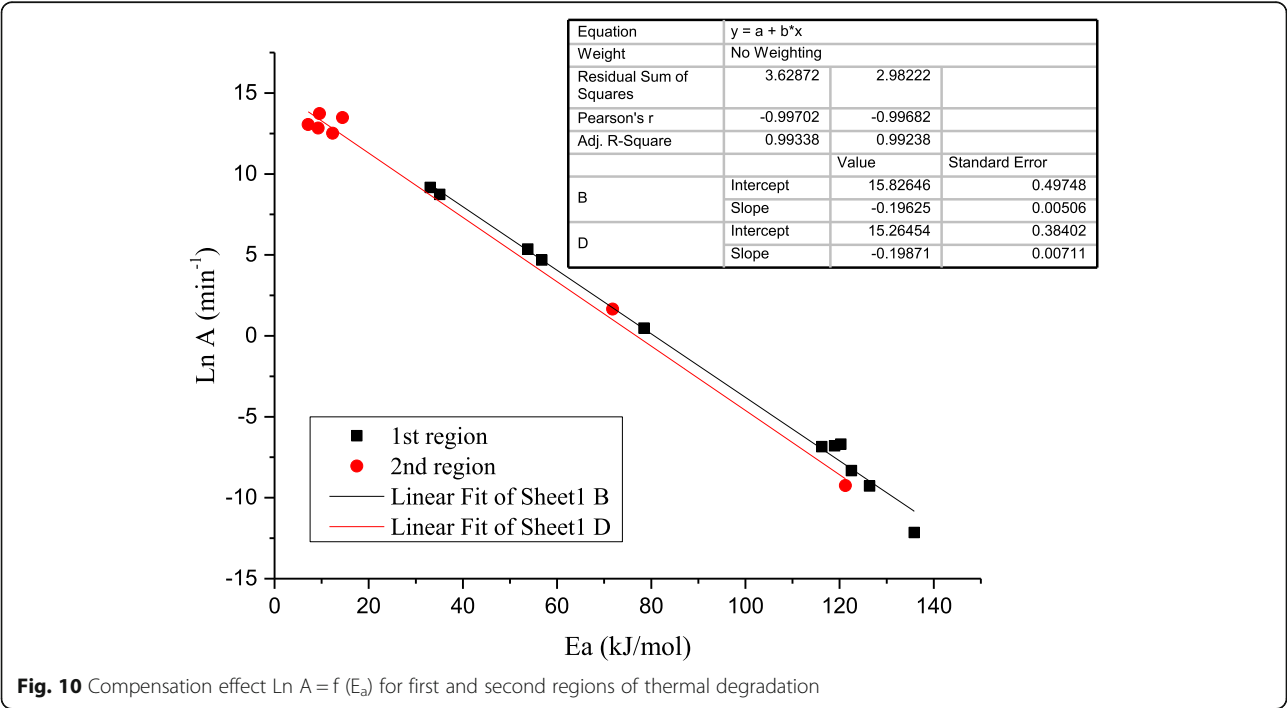


Table 3 Thermal kinetic results for bulk aluminum oxide pyrolysis

MD	1st region			2nd region		
	Ea (kJ.mol ⁻¹)	R ²	Ln A (min ⁻¹)	Ea (kJ.mol ⁻¹)	R ²	Ln A (min ⁻¹)
F1	122.537	0.95148	-8.323	9.262	0.84556	12.832
F0	116.238	0.94047	-6.845	0.259	0.00617	11.554
F2	126.387	0.97401	-9.275	71.801	0.88681	1.649
F3	135.861	0.9674	-12.151	121.250	0.89997	-9.252
R2	118.969	0.94747	-6.793	9.561	0.96141	13.728
R3	120.262	0.94866	-6.691	14.454	0.94953	13.479
P3	33.097	0.91717	9.164	-6.984	0.97796	-
D3	78.465	0.9505	0.470	12.347	0.9151	12.515
P2	53.789	0.93044	5.355	-5.219	0.94073	-
A2	56.764	0.94564	4.686	7.154	0.837	13.051
A3	35.1	0.93365	8.740	1.373	0.29837	12.596



Abbreviations

TGA: Thermogravimetric analysis; f (a): Represents the mode of degradation of the substance; g (a): Integral form of the function f(a); A: Pre-exponential factor [min^{-1}]; E: Apparent activation energy [KJ.mol^{-1}]; k: Reaction rate constant [min^{-1}]; m_0 : Initial weight of the sample, [mg]; m_t : Weight of the sample at the particular temperature T [mg]; m_{∞} : Weight at the end of degradation step [mg]; β : Heating rate [$^{\circ}\text{C.min}^{-1}$]; R: Constante des gaz parfait [$\text{J.mol}^{-1}.\text{K}^{-1}$]; T: Absolute temperature [K]; T_0 : Initial température [K]; t: Time [min]; n: Reaction order; α : Conversion rate

Acknowledgments

This work was completed in the ELTE Institutional Excellence Program (1783-3/2018/FEKUTSRAT) supported by the Hungarian Ministry of Human Capacities. Open access funding provided by Eötvös Loránd Eötvös University (ELTE).

Authors' contributions

The authors read and approved the final manuscript.

Funding

Not applicable.

Availability of data and materials

The authors declare that the availability of data and materials.

Declarations

Competing interests

The authors declare that they have no competing interests.

Author details

¹Doctoral School of Environmental Sciences, Eötvös Loránd University, Budapest H-1117, Hungary. ²Department of Chemistry, Hafr Al-Batin University, Hafar Al Batin, Saudi Arabia. ³Institute of Chemistry, Eötvös Loránd University, Budapest H-1117, Hungary.

Received: 27 January 2021 Accepted: 25 October 2021

Published online: 02 December 2021

References

1. Bagheri Khatibani, A., Rozati, S.M.: Synthesis and characterization of amorphous aluminum oxide thin films prepared by spray pyrolysis: effects of substrate temperature. *J. Non-Cryst. Solids*. **363**, 121–133 (2013). <https://doi.org/10.1016/j.jnoncrysol.2012.12.013>
2. Isac, L., Duta, A., Purghel, E., Chitanu, G.C., Mitrea, S., Pelin, I.: Tailoring alumina thin film properties using hydrophilic/hydrophobic copolymer additives. *Phys. Status Solidi Appl. Mater. Sci.* **205**(10), 2413–2416 (2008). <https://doi.org/10.1002/pssa.200779429>
3. Smet, P.F., Lauwaert, J., Avci, N., Poelman, D., Vrielinck, H.: Optical and structural properties of aluminium oxide thin films prepared by a non-aqueous sol-gel technique. *J. Sol-Gel Technol.* **59**(2), 327–333 (2011). <https://doi.org/10.1007/s10971-011-2505-9>
4. X. Nie, E.I. Meletis, J.C. Jiang, A. Leyland, A.L. Yerokhin, A. Matthews, Abrasive wear/corrosion properties and TEM analysis of Al₂O₃ coatings fabricated using plasma electrolysis. *Surf. Coatings Technol.* **149** (2002) 245–251. [https://doi.org/10.1016/S0257-8972\(01\)01453-0](https://doi.org/10.1016/S0257-8972(01)01453-0), 2–3
5. Wang, Y., Lim, S., Luo, J.L., Xu, Z.H.: Tribological and corrosion behaviors of Al₂O₃/polymer nanocomposite coatings. *Wear*. **260**(9–10), 976–983 (2006). <https://doi.org/10.1016/j.wear.2005.06.013>
6. Boström, T., Westin, G., Wäckelgård, E.: Optimization of a solution-chemically derived solar absorbing spectrally selective surface. *Sol. Energy Mater. Sol. Cells*. **91**(1), 38–43 (2007). <https://doi.org/10.1016/j.solmat.2006.07.002>
7. Cui, J., Kast, M.G., Hamman, B.A., Afriyie, Y., Woods, K.N., Plassmeyer, P.N., Perkins, C.K., Ma, Z.L., Kesler, D.A., Page, C.J., Boettcher, S.W., Hayes, S.E.: Aluminum oxide thin films from aqueous solutions: insights from solid-state NMR and dielectric response. *Chem. Mater.* **30**(21), 7456–7463 (2018). <https://doi.org/10.1021/acs.chemmater.7b05078>
8. Yu, B.-G., Shin, C.H., Lee, H.C., Cha, S.Y., Kwak, D.-H., Lee, W.-J.: Fabrication and characterization of MFISFET using Al₂O₃ insulating layer for non-volatile memory. *Integr. Ferroelectr.* **34**(1–4), 113–120 (2007). <https://doi.org/10.1080/10584580108012880>
9. J. Gottmann, E.W. Kreutz, Pulsed laser deposition of alumina and zirconia thin films on polymers and glass as optical and protective coatings. *Surf. Coatings Technol.* **116–119** (1999) 1189–1194. [https://doi.org/10.1016/S0257-8972\(99\)00191-7](https://doi.org/10.1016/S0257-8972(99)00191-7)
10. Vitanov, P., Harizanova, A., Ivanova, T., Dimitrova, T.: Chemical deposition of Al₂O₃ thin films on Si substrates. *Thin Solid Films*. **517**(23), 6327–6330 (2009). <https://doi.org/10.1016/j.tsf.2009.02.085>
11. Plóciennik, P., Guichaoua, D., Korcala, A., Zawadzka, A.: Studies of aluminum oxide thin films deposited by laser ablation technique. *Opt. Mater. (Amst)*. **56**, 49–57 (2016). <https://doi.org/10.1016/j.optmat.2016.01.060>
12. Yang, H., Liu, M., Ouyang, J.: Novel synthesis and characterization of nanosized γ -Al₂O₃ from kaolin. *Appl. Clay Sci.* **47**(3–4), 438–443 (2010). <https://doi.org/10.1016/j.clay.2009.12.021>
13. Balakrishnan, G., Kuppasami, P., Sundari, S.T., Thirumurugesan, R., Ganesan, V., Mohandas, E., Sastikumar, D.: Structural and optical properties of γ -alumina thin films prepared by pulsed laser deposition. *Thin Solid Films*. **518**(14), 3898–3902 (2010). <https://doi.org/10.1016/j.tsf.2009.12.001>
14. Blittersdorf, S., Bahlawane, N., Kohse-Höinghaus, K., Atakan, B., Müller, J.: CVD of Al₂O₃ thin films using aluminum tri-isopropoxide. *Chem. Vap. Depos.* **9**(4), 194–198 (2003). <https://doi.org/10.1002/cvde.200306248>
15. Hwang, Y., Heo, K., Chang, C.H., Joo, M.K., Ree, M.: Synchrotron X-ray reflectivity study of high dielectric constant alumina thin films prepared by atomic layer deposition. *Thin Solid Films*. **510**(1–2), 159–163 (2006). <https://doi.org/10.1016/j.tsf.2005.12.162>
16. Cibert, C., Hidalgo, H., Champeaux, C., Tristant, P., Tixier, C., Desmaison, J., Catherinot, A.: Properties of aluminum oxide thin films deposited by pulsed laser deposition and plasma enhanced chemical vapor deposition. *Thin Solid Films*. **516**(6), 1290–1296 (2008). <https://doi.org/10.1016/j.tsf.2007.05.064>
17. Boidin, R., Halenkovič, T., Nazabal, V., Beneš, L., Němec, P.: Pulsed laser deposited alumina thin films. *Ceram. Int.* **42**(1), 1177–1182 (2016). <https://doi.org/10.1016/j.ceramint.2015.09.048>
18. Dhonge, B.P., Mathews, T., Sundari, S.T., Thinaharan, C., Kamruddin, M., Dash, S., Tyagi, A.K.: Spray pyrolytic deposition of transparent aluminum oxide (Al₂O₃) films. *Appl. Surf. Sci.* **258**(3), 1091–1096 (2011). <https://doi.org/10.1016/j.susc.2011.09.040>
19. Adamopoulos, G., Thomas, S., Bradley, D.D.C., McLachlan, M.A., Anthopoulos, T.D.: Low-voltage ZnO thin-film transistors based on Y₂O₃ and Al₂O₃ high- k dielectrics deposited by spray pyrolysis in air. *Appl. Phys. Lett.* **98**(12), 2009–2012 (2011). <https://doi.org/10.1063/1.3568893>
20. Ienei, E., Isac, L., Duță, A.: Synthesis of alumina thin films by spray pyrolysis. *Rev. Roum. Chim.* **55**, 161–165 (2010)
21. Khanna, A., Bhat, D.G., Harris, A., Beake, B.D.: Structure-property correlations in aluminum oxide thin films grown by reactive AC magnetron sputtering. *Surf. Coatings Technol.* **201**(3–4), 1109–1116 (2006). <https://doi.org/10.1016/j.surfcoat.2006.01.033>
22. Gianneta, V., Nassiopoulou, A.G., Krontiras, C.A., Georga, S.N.: Porous anodic alumina thin films on Si: Interface characterization. *Phys. Status Solidi Curr. Top. Solid State Phys.* **5**(12), 3686–3689 (2008). <https://doi.org/10.1002/pssc.200780160>
23. Wang, T., Pu, J., Bo, C., Jian, L.: Sol-gel prepared Al₂O₃ coatings for the application as tritium permeation barrier. *Fusion Eng. Des.* **85**(7–9), 1068–1072 (2010). <https://doi.org/10.1016/j.fusengdes.2010.01.021>
24. Vanbesien, K., De Visschere, P., Smet, P.F., Poelman, D.: Electrical properties of Al₂O₃ films for TFEL-devices made with sol-gel technology. *Thin Solid Films*. **514**(1–2), 323–328 (2006). <https://doi.org/10.1016/j.tsf.2006.02.034>
25. Moubah, R., Colis, S., Leuvrey, C., Schmerber, G., Drillon, M., Dinia, A.: Synthesis and characterization of Ca₃Co₄O₉ thin films prepared by sol-gel spin-coating technique on Al₂O₃ (001). *Thin Solid Films*. **518**(16), 4546–4548 (2010). <https://doi.org/10.1016/j.tsf.2009.12.027>
26. Ferrari, V.C., Dupim, I.S., Sousa, V., Souza, F.L.: Photoactive multilayer WO₃ electrode synthesized via dip-coating. *Ceram. Int.* **44**(18), 22983–22990 (2018). <https://doi.org/10.1016/j.ceramint.2018.09.097>
27. Farid, R., Rajan, K., Sarkar, D.K.: Enhanced corrosion protection of aluminum by ultrasonically dip coated sodium silicate thin films. *Surf. Coatings Technol.* **374**, 355–361 (2019). <https://doi.org/10.1016/j.surfcoat.2019.05.082>
28. Zelcer, A., Saleh Medina, L.M., Hoijemberg, P.A., Fuentes, M.C.: Optical quality mesoporous alumina thin films. *Microporous Mesoporous Mater.* **287**, 211–219 (2019). <https://doi.org/10.1016/j.micromeso.2019.05.006>
29. Redfern J.P. "Thermogravimetric Analysis," *Analyst*, vol. 88, no. 1053, pp. 906–924, 1963.

30. Bouzbib, M., Pogonyi, A., Kolonits, T., Vida, Á., Dankházi, Z., Sinkó, K.: Sol – gel alumina coating on quartz substrate for environmental protection. *J. Sol-Gel Sci. Technol.* **93**(2), 262–272 (2020). <https://doi.org/10.1007/s10971-019-05193-y>
31. Chandradass, J., Bae, D.S.: Synthesis and characterization of alumina nanoparticles by Igepal CO-520 stabilized reverse micelle and sol-gel processing. *Mater. Manuf. Process.* **23**(5), 494–498 (2008). <https://doi.org/10.1080/10426910802104211>
32. Criado J.M, Malek J., Ortega A., "APPLICABILITY OF THE MASTER PLOTS IN KINETIC ANALYSIS," *Thermochim. Acta*, vol. 147, no. 2, pp. 377–385, 1989.
33. Villanueva M., "Thermogravimetric study of the decomposition process of the system," *Polymer*, vol. 41, no. 12, pp. 4635–4641, 2000.
34. Dickinson, C.F., Heal, G.R.: *Thermochimica Acta A review of the ICTAC Kinetics Project , 2000 Part 1. Isothermal Results.* **494**(1-2), 1–14 (2009). <https://doi.org/10.1016/j.tca.2009.05.003>
35. Bustamante, L., Rogaume, T., Guillaume, E.: Analysis of Principal Gas Products During Combustion of Polyether Polyurethane Foam at Different Irradiance Levels. 933–940 (2009). <https://doi.org/10.1016/j.firesaf.2009.05.003f>
36. Avrami, M.: Kinetics of Phase Change. I Gen. Theory. **1103**, (1939). <https://doi.org/10.1063/1.1750380>
37. Liu, F., Lai, Y., Liu, J., Wang, B., Kuang, S., Zhang, Z., Li, J., Liu, Y.: Characterization of chemical bath deposited CdS thin films at different deposition temperature. *J. Alloys Compd.* **493**(1-2), 305–308 (2010). <https://doi.org/10.1016/j.jallcom.2009.12.088>
38. Van Lare, C., Lenzmann, F., Verschuuren, M.A., Polman, A.: Dielectric scattering patterns for efficient light trapping in thin-film solar cells. *Nano Lett.* **15**(8), 4846–4852 (2015). <https://doi.org/10.1021/nl5045583>
39. Hu, B., Jia, E., Du, B., Yin, Y.: A new sol-gel route to prepare dense Al₂O₃ thin films. *Ceram. Int.* **42**(15), 16867–16871 (2016). <https://doi.org/10.1016/j.ceramint.2016.07.181>
40. Barrie, P.J.: The mathematical origins of the kinetic compensation effect: 1. the effect of random experimental errors. *Phys. Chem.* **14**, 318–326 (2012). <https://doi.org/10.1039/c1cp22666e>

Publisher's Note

Springer Nature remains neutral with regard to jurisdictional claims in published maps and institutional affiliations.

Submit your manuscript to a SpringerOpen[®] journal and benefit from:

- Convenient online submission
- Rigorous peer review
- Open access: articles freely available online
- High visibility within the field
- Retaining the copyright to your article

Submit your next manuscript at ► [springeropen.com](https://www.springeropen.com)